Stanford Exploration Project, Report 72, December 18, 1997, pages 1–125

Stanford Exploration Project, Report 72, December 18, 1997, pages 1–125

Angle-dependent reflectivity from elastic reverse-time migration

Carlos A. Cunha Filho[1]

keywords: *reflectivity, modeling, imaging, elastic, anisotropy, diffraction*

ABSTRACT

Any amplitude-based lithologic inversion method must compensate for all changes in the amplitudes that are not directly related to the properties to be estimated. Conventional methods for compensation of geometrical spreading and transmission/conversion losses are not applicable when the subsurface structures cannot be well approximated by horizontal layers. Migration-based methods have been proposed recently as a solution for correctly retrieving angle dependent reflectivity in the presence of complex structures. I this paper I describe here an anisotropic prestack reverse migration scheme for retrieving the P–P reflectivity as a function of the local Snell parameter. The paper shows that this functionality represents a more appropriate way of expressing the directional dependence of the reflection coefficient than the more usual angular function.

INTRODUCTION

Different methods for retrieving the angle-dependent reflection coefficient from surface seismic data have been described in the geophysical literature. In a classic paper, O'Doherty and Anstey (1971) analyzed the relative importance of a large number of factors in the final amplitude of the recorded reflections. Any inversion method that intends to retrieve rock properties from amplitude information must compensate for all the factors that are not directly related to such properties. This study focuses on those factors that are affected by the long wavelength elastic characteristics of the medium, that is, geometrical spreading and transmission/conversion losses.

Initial methods for recovering the angle-dependent reflectivity function were based on the assumption that the Earth can be considered as plane-layered within the range covered by a common midpoint gather (CMP), which is the basic assumption of standard CMP processing (Newman, 1973; Yu, 1985; Kolb and Chapel, 1989; Cunha, 1990). Although these methods properly compensate for the long wavelength losses

[1]**email:** not available

in a reasonable number of practical problems, they cannot be applied to areas with structurally complex geology.

Recently, some more powerful methods for angle-dependent reflectivity recovery, based in migration algorithms, have been developed. De Bruin et al. (1990a) presented a method for estimation of the angle-dependent reflectivity using a scalar pre-stack phase-shift migration scheme. Tests with synthetic data showed that the method was able to retrieve the reflectivity function with considerable accuracy for horizontal layers, but when dip was present (de Bruin, 1990b) the retrieved function was incorrectly shifted, because of the assumption of a horizontally-layered earth, which is implicit in their imaging principle (integration along constant Snell parameter traces). Lumley and Beydoun (1991) introduced a different scheme for retrieving the reflectivity function, using an elastic pre-stack Kirchhoff migration scheme. Their imaging principle was not limited by the horizontal layer assumption and was successfully applied to synthetic and real data. Both approaches, however, are limited to the assumptions that the medium is isotropic medium, and the wavefields are decomposable.

This paper describes a method for retrieving the angle-dependent reflectivity that is based on anisotropic prestack reverse time migration. Reverse time migration was independently developed in the early 1980s by Whitmore (1983), Baysal et al. (1983), McMechan (1983), and Lowental and Mufty (1983). Levin (1984) gives a general discussion of the different formulations, clarifies the principle of reverse time migration and shows how it relates to depth extrapolation methods. Karrenbach (1991) developed an anisotropic reverse-time migration/inversion scheme using a tensorial imaging condition represented by the crosscorrelation between the different components of the upcoming and downgoing wavefields. Each of the resulting images is associated with a different component of the stiffness tensor. His approach is equivalent to the first step of a linearized inverse algorithm because the residuals between the modeled and recorded wavefields at the surface, rather than just the recorded wavefield, were propagated backward in time. As a result, the images were directly related to perturbations in the impedance, instead of to the reflectivity functions.

Similarly to the work developed by Karrenbach, the method described in this paper uses an anisotropic prestack, reverse-time migration algorithm. However, I use a different modeling scheme, which is based on the equivalent medium theory (Cunha, 1991), and an alternative approach for the surface boundary conditions. Instead of the tensorial imaging principle, this method uses the usual scalar imaging principle and an additional imaging condition to estimate the reflection angle associated with the imaged reflectivity.

OVERVIEW OF THE MIGRATION SCHEME

The reverse time migration scheme described in this paper can be divided into the following three steps:

step 1

This step evaluates the spatial operators using a spatially smooth stiffness-density model ($C_{11}, C_{33}, C_{13}, C_{55}$, and ρ). It is worthwhile to note that all spatial derivatives of the elastic parameters are calculated only once, instead of for each time step of each shot record.

The next steps are performed **for each shot record**.

step 2

Forward time modeling of the particle-displacement $\mathbf{u}$ and particle-velocity $\dot{\mathbf{u}}$ wavefields, up to the end time of the shot record. **For each time step** the following arrays are computed for use in the third step:

- Scalar downgoing particle-displacement field

$$u(x, z, t) = \mathrm{sign}(\dot{u}_z)\sqrt{\dot{u}_x^2 + \dot{u}_z^2}$$

- Unit vector in the group propagation direction of the downgoing wavefield

$$\hat{\mathbf{i}}(x, z, t).$$

This step also computes the total "energy," at each grid point

$$E(x, z) = \int u^2(x, z, t)\, dt.$$

The modeling is implemented with the elastic modeling scheme described in another paper included in this report (Cunha, 1991). Because the imaging step requires access to the time slices generated in this step in the reverse time sequence, this step cannot be performed simultaneously with step 3. Since the three modeling cubes are too large to be held in core memory, we are left with two options for solving this problem: to store the cubes in an auxiliary file to be read in reverse order in step 3, or to keep only the last time slice and do reverse time propagation simultaneously with the third step. In the scheme presented here, I use the first option not only because it will have a better performance if a data vault is available, but also because it will not be affected by the absorbing boundary or the extra dispersion caused by the backward propagation.

step 3

Backward time propagation of the recorded particle-displacement field and $\mathbf{w}$ and its time-derivative $\dot{\mathbf{w}}$, starting at the end time of the shot record and ending at time zero.

These wavefields are introduced as time-dependent boundary conditions at $z = 0$. Simultaneously with this backward propagation, this step also computes the lag zero of the correlation between the downgoing scalar field $u(x, z)$ and the upcoming scalar field $w(x, z)$. **For each time step** the following arrays are computed:

- Scalar upcoming particle-displacement field

$$w(x, z, t) = \mathrm{sign}(\dot{w}_z)\sqrt{\dot{w}_x^2 + \dot{w}_z^2}$$

- Unit vector in the group propagation direction of the upcoming wavefield

$$\hat{\mathbf{r}}(x, z, t).$$

Finally, the reflection coefficient image is computed as

$$\begin{aligned}\Psi(x, z) &= \frac{\int u(x, z, t) w(x, z, t)\, dt}{E(x, z)}, \quad \text{where } E(x, z) \geq E_{cut}, \\ \Psi(x, z) &= \frac{\int u(x, z, t) w(x, z, t)\, dt}{E_{cut}}, \quad \text{elsewhere,}\end{aligned}$$

and the local Snell parameter image as

$$\breve{p}(x, z) = \frac{\int \mid u(x, z, t) w(x, z, t) \mid \tilde{p}(x, z, t)\, dt}{\int \mid u(x, z, t) w(x, z, t) \mid\, dt},$$

where $\tilde{p}(x, z, t)$ is computed from $\hat{\mathbf{i}}$ and $\hat{\mathbf{r}}$, as described in the next section.

IMAGING CONDITION AND LOCAL SNELL PARAMETER

Imaging condition for the reflection coefficient

Migration includes two distinct steps: downward extrapolation in depth or backward extrapolation in time, and imaging for the desired attribute. When the desired attribute is the reflectivity, Claerbout's imaging principle (Claerbout, 1971) represents the basis for many imaging condition equations. According to this principle, a reflector exists at a point where the upcoming and the downgoing wavefields coincide in time and space.

Jacobs (1982) compared three different ways to implement this principle in prestack profile migration in the $\omega - x$ domain:

$$c_1 = \int U D^*\, d\omega, \qquad c_2 = \int U \frac{D^*}{\mid D \mid}\, d\omega, \qquad c_3 = \int U \frac{D^*}{\mid D \mid^2 + \epsilon}\, d\omega. \quad (1)$$

His conclusion was that c_3, though theoretically more correct for estimating the reflection coefficient, was too noise sensitive to be used in that migration scheme. Hildebrand (1987) used a variation of this principle to image for the acoustic impedance rather than the reflection coefficient, using reverse-time migration to extrapolate the pressure and particle-velocity wavefields.

Most imaging methods described in the literature involve the correlation between scalar wavefields. An exception is the tensorial imaging condition formulated by Karrenbach (1991):

$$c_{jklm} = \int \partial_m(U_l)\partial_k(D_j)\, dt,$$

where c_{jklm} can be interpreted as the reflectivity function associated with the corresponding stiffness component.

Although this equation gives a more complete picture of the subsurface, I decided to focus attention on the $P-P$ reflectivity by using a scalar imaging condition similar to c_3 in equation (1):

$$\begin{aligned} \Psi(x,z) &= \frac{\int u(x,z,t)w(x,z,t)\,dt}{E(x,z)}, \quad \text{where } E(x,z) \geq E_{cut} \\ \Psi(x,z) &= \frac{\int u(x,z,t)w(x,z,t)\,dt}{E_{cut}}, \quad \text{elsewhere.} \end{aligned} \tag{2}$$

Equation (2) gives the correct estimation of the reflection coefficient in the regions well illuminated by the source ($E(x,z) \geq E_{cut}$) and a damped estimation in the dim regions.

Computation of the local snell parameter

Inversion methods which use the directional dependence of the reflection coefficient to estimate the elastic parameters of the medium (AVO inversion) use in general an angular functionality to express such a dependence. This choice is not the more convenient because the angle estimation is strongly dependent on the macro model that was used in the estimation process. Moreover, the propagation angles depend on the elastic perturbations that it is been used to estimate. A more appropriate choice for expressing the directional dependence of the reflection coefficient is the *local Snell parameter*, which is defined as the component of the slowness parallel to the "reflector plane" at each position of the underground. Evidently, not all points of the subsurface can be considered as a reflector, but at all points of interest; that is, where the the upcoming wavefronts intercepts the downgoing wavefront, a "reflector plane can be defined". As defined, the local Snell parameter is conserved for any perturbation in the local elastic parameters. Although its estimated value will be still dependent on the macro model, it will be much less sensitive to errors in the model than the angle.

Figure **??** shows a descending (incident) wavefield crossing an ascending (reflected) wavefield at a given time step of the backward propagation part of the scheme. The crossing point defines the point of the interface that was imaged at that time, and the

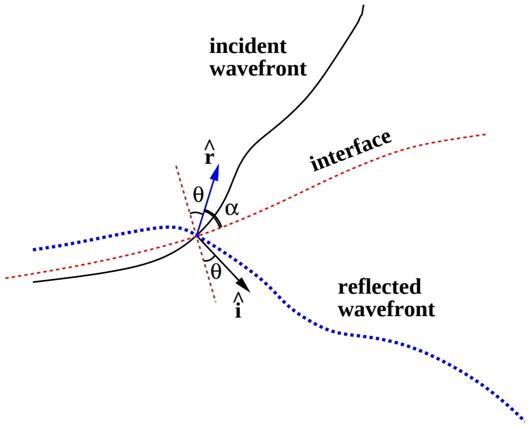

Figure 1: The points where the ascending and descending wavefronts overlap define the location of the reflector. The reflection angle can be determined by the gradients of the two wavefields at the reflection point, at the time when the reflection occurred. carlos4-reflect [NR]

angles α and βi are measured, respectively, from the tangent and from the normal to the interface at that point.

From the figure we get the following relation,

$$\cos(2\alpha) = \hat{\mathbf{i}} \cdot \hat{\mathbf{r}},$$

where the *unit vectors* $\hat{\mathbf{i}}$ and $\hat{\mathbf{r}}$ represent, respectively, the directions of incidence and reflection. I define the *local Snell parameter* $\tilde{p}$ as the slowness component parallel to the interface at the reflection point

$$\tilde{p} \quad = \quad \frac{\sin(\theta)}{V_p} \quad = \quad \sqrt{\frac{\hat{\mathbf{i}} \cdot \hat{\mathbf{r}} + 1}{2V_p^2}}, \tag{3}$$

where V_p is the P wave group velocity at that particular location. This definition is restricted to an isotropic assumption, but a more general definition can be formulated that includes the anisotropic extension of Snell's law.

The unit vectors $\hat{\mathbf{i}}$ and $\hat{\mathbf{r}}$ are estimated from the particle velocity field, by using the following equations:

$$\begin{aligned} \hat{\mathbf{i}} \quad &= \quad \mathrm{sign}(\frac{\partial v^d}{\partial t})\frac{\nabla v^d}{\mid \nabla v^d \mid}, \\ \hat{\mathbf{r}} \quad &= \quad \mathrm{sign}(\frac{\partial v^u}{\partial t})\frac{\nabla v^u}{\mid \nabla v^u \mid}, \end{aligned} \tag{4}$$

where v^d and v^u are, respectively, the downgoing and the upcoming scalar particle velocity wavefields, defined by the equation

$$\begin{aligned} v^d \quad &= \quad \mathrm{sign}(\dot{u}_z)\sqrt{\dot{u}_x^2 + \dot{u}_z^2} \\ v^u \quad &= \quad \mathrm{sign}(\dot{w}_z)\sqrt{\dot{w}_x^2 + \dot{w}_z^2}. \end{aligned}$$

The sign of the time derivative in equation (4) is calculated by

$$\mathrm{sign}(\frac{\partial v^d}{\partial t}) = \frac{\partial \mathrm{sign}(\dot{u}_z)}{\partial t}\sqrt{\dot{u}_x^2 + \dot{u}_z^2} + \mathrm{sign}(\dot{u}_z)\frac{\partial\sqrt{\dot{u}_x^2 + \dot{u}_z^2}}{\partial t}$$

which results in

$$\mathrm{sign}(\frac{\partial v^d}{\partial t}) = \mathrm{sign}(\dot{u}_z)\mathrm{sign}(\dot{\mathbf{u}}\frac{\partial \dot{\mathbf{u}}}{\partial t}).$$

A SYNTHETIC EXAMPLE

A synthetic dataset comprising a hundred shot gathers was generated with the modeling scheme described in Cunha (1991). The model includes isotropic and transverse isotropic layers, which are described at each point by five parameters ($c_{11}, c_{33}, c_{13}, c_{55}$, and ρ). Figure **??** shows the c_{11} component of the model, while Figure **??** shows the 2 components of the recorded wavefield for one shot.

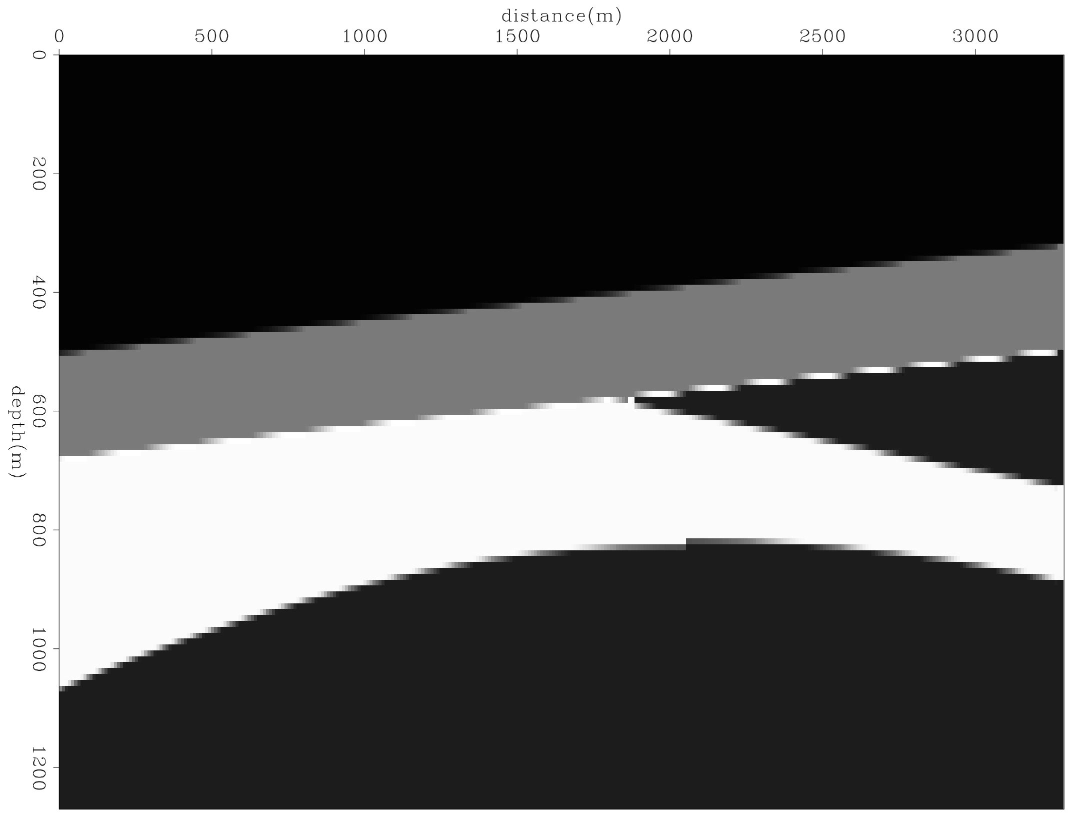

Figure 2: The c_{11} stiffness component of the synthetic structural model used to generate the data of Figure **??**. The model includes isotropic and transverse isotropic layers. carlos4-syntmodel [ER]

A migrated shot gather and the result of stacking all the migrated shot gathers are shown in Figure **??**. The low resolution around the horizontal position of 2000 meters was caused by the accidental missing of twenty consecutives migrated shot gathers, sufficiently close to the report dead line. The acquisition geometry was off-end, with receivers at the right of the source.

The retrieved angle-dependent reflectivity at one of the reflectors is compared in

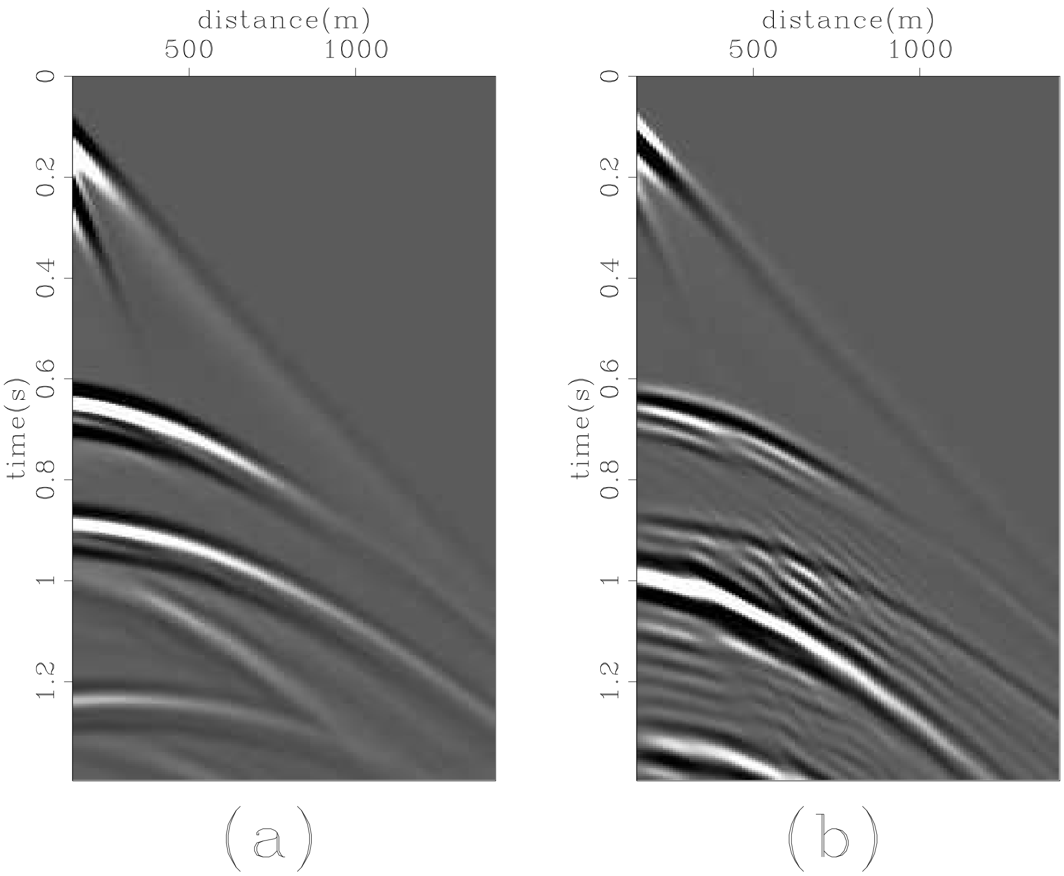

Figure 3: One of the synthetic shot records generated by finite differences elastic modeling. *(a)* Is the vertical component of the displacement field recorded at the surface. *(b)* Is the horizontal component of the same field. The relative weakness of the shallow reflection at large offsets is caused by the introduction of a thin absorbing region near the free surface in order to simulate a low Q, unconsolidated sediment. Click the button to see a movie with every tenth shot gather. The first set is the z component and the second set is the x component. carlos4-dataslice [ER]

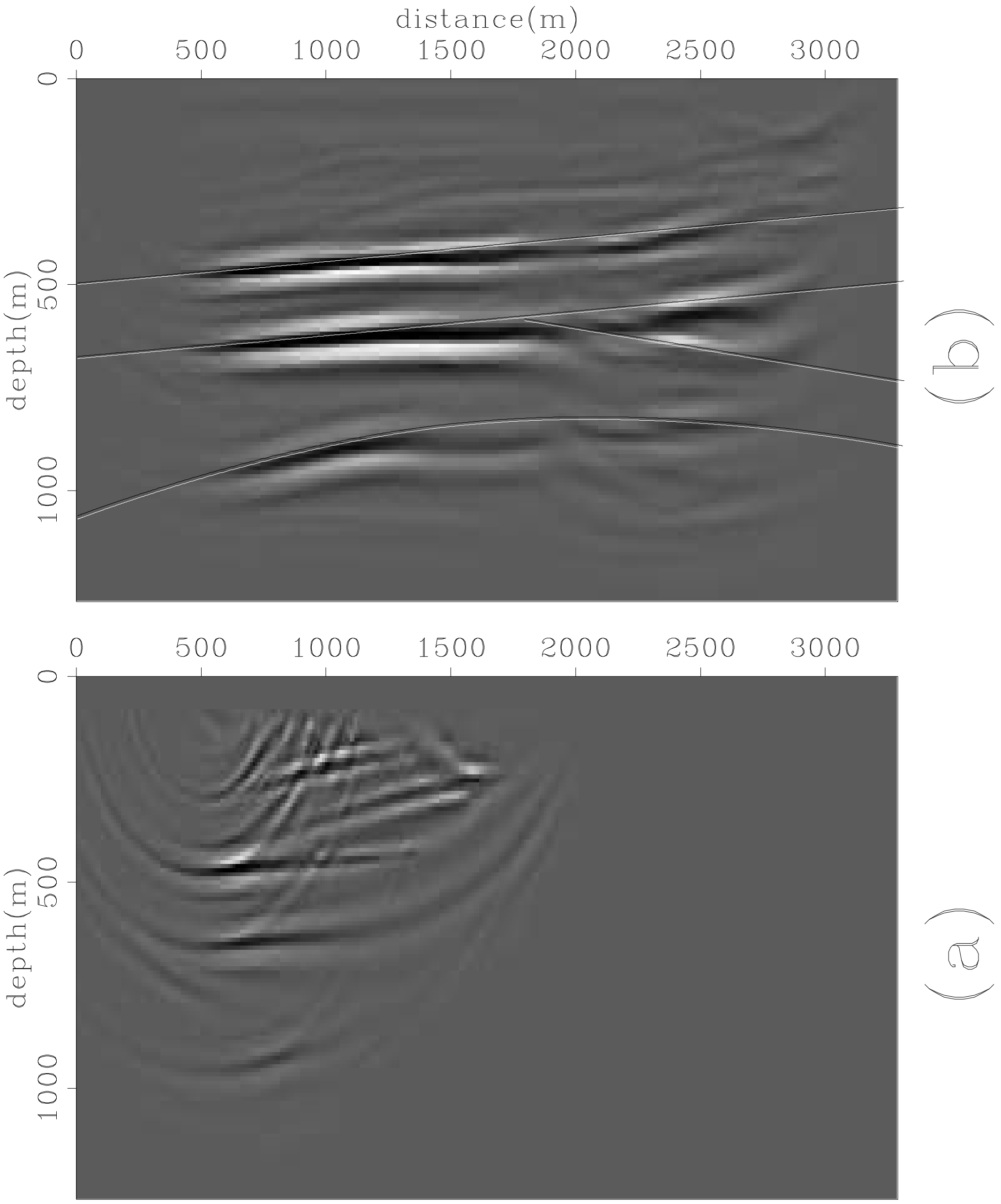

Figure 4: *(a)* Migrated image of one shot gather. *(b)* Stacking of the migrated shot gathers.The interfaces of the correct model are overlaid to the stacked session. carlos4-migimag [ER]

Figure **??** to the theoretical reflectivity function. Although the retrieved reflectivity function fits the general trend of the theoretical curve, it is clear that the method still needs some refinement to allow its application to real data.

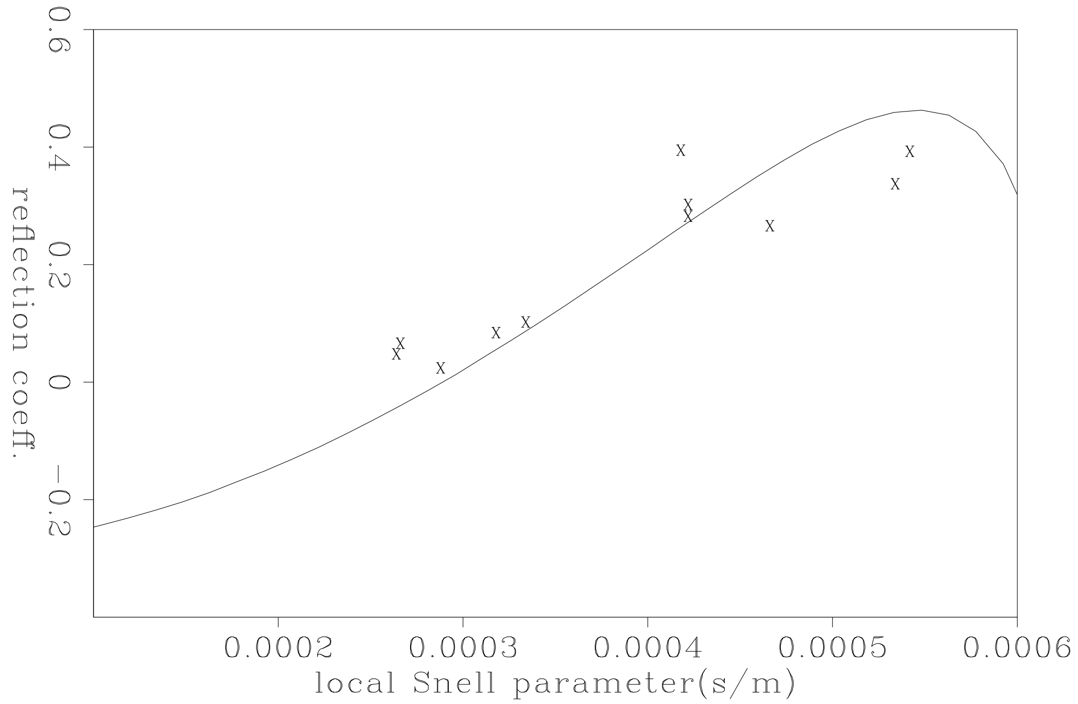

Figure 5: The X represent the retrieved reflectivity as a function of the local Snell parameter and the continuous line, the theoretical reflectivity function carlos4-refofp [ER]

CONCLUSIONS

In structurally complex media, the accurate recovery of the angle-dependent reflectivity function requires the use of an elastic prestack migration technique. If, in addition to structural complexity, the medium has a relevant degree of anisotropy, a more sophisticated imaging scheme that incorporates wave propagation in an anisotropic media must be used. I described a method for recovery of the angle-dependent reflectivity that fulfills those requirements. The method is based on an anisotropic reverse-time migration algorithm, which simultaneously images for the reflectivity and the reflection angle. Preliminary results obtained with synthetic data show the viability of the method. However, some refinement is still required before it can be applied to real data.

REFERENCES

Baysal, E., Kosloff, D.D., and Sherwood, J.W.C., 1983, Reverse time migration: Geophysics, **48**, 1514–1524.

Claerbout, J.F., 1971, Toward a unified theory of reflector mapping: Geophysics, **36**, 467–481.

Cunha, C.A., 1990, Snell-beam transform: Retrieving the angle-dependent reflectivity: Presented at the 60th Ann. Internat. Mtg., Soc. Expl. Geophys., Expanded Abstracts, 1507–1510.

Cunha, C.A., 1991, Accurate, efficient 2-D elastic modeling using S&M: Geophysics, **72**, 101–110.

de Bruin, C.G.M., Wapenar, C.P.A., and Berkhout, A.J., 1990a: Angle-dependent reflectivity by means of prestack migration: Geophysics, **55**, 1223–1234.

de Bruin, C.G.M., Wapenar, C.P.A., and Berkhout, A.J., 1990b: Imaging for angle-dependent reflectivity in the presence of dip: Presented at the 60th Ann. Internat. Mtg., Soc. Expl. Geophys., Expanded Abstracts, 1503–1506.

Hildebrand, S.A., 1987, Reverse-time depth migration: Impedance imaging condition: Geophysics, **52**, 1060–1064.

Jacobs, A., 1982, The pre-stack migration of profiles: PhD thesis, Stanford University. Also SEP–**34**.

Karrenbach, M., 1991, Prestack reverse-time migration in anisotropic media: SEP–**70**, 113–121.

Kolb, P., and Chapel, F., 1989, Lithologic inversion: A reflectivity versus angle (RVA) approach: Presented at the 60th Ann. Internat. Mtg., Soc. Expl. Geophys., Expanded Abstracts, 695–699.

Levin, S., 1984, Principle of reverse-time migration: Geophysics, **49**, 581–583.

Lumley, D.E., and Beydoun, W.B., 1991, Elastic parameter estimation by Kirchhoff prestack depth migration/inversion: SEP–**70**, 165–192.

Newman, P., 1973, Divergence effects in a layered earth: Geophysics, **38**, 481–488.

O'Doherty, R.F., and Anstey, N.A., 1971, Reflections on amplitudes: Geophysical Prospecting, **19**, 430–458.

Uren, N.F., Gardner, G.H.F., and McDonald, J.A., 1990, The migrator's equation for anisotropic media: Geophysics, **55**, 1429–1434.

Yu, G., 1985, Offset-amplitude variation and controlled-amplitude processing: Geophysics, **50**, 2697–2708.